Control Engineering Practice 21 (2013) 1519–1530

Contents lists available at ScienceDirect

Control Engineering Practice

journal homepage: www.elsevier.com/locate/conengprac

Design and application of a sliding mode controller for accurate motion synchronization of dual servo systems

Burak Sencer [a,*], Tatsuya Mori [b], Eiji Shamoto [c]

[a] Department of Mechanical Science and Engineering, Graduate School of Engineering, Nagoya University, Furo-cho, Chikusa-ku, Building 2, 2F Room 205, Nagoya 464-8603, Japan
[b] Daido Amistar Co., Ltd., 3-152 Hino, Daito-city, Osaka 574-0061, Japan
[c] Nagoya University, Furo-cho, Chikusa-ku, Building 2, 2F, Room 202, Nagoya 464-8603, Japan

ARTICLE INFO

Article history:
Received 19 October 2012
Accepted 7 July 2013

Keywords:
Servo system
Synchronization
Tracking error
Sliding mode control
Double-sided milling

ABSTRACT

This paper presents a continuous time sliding mode controller (SMC) design to deal with the problem of motion synchronization in dual spindle servo systems. Synchronization error is defined as the differential position error between the two servo drives that follow identical reference motion trajectory. Proposed SMC controller penalizes three error states; namely individual axis tracking errors and the synchronization error for accurate synchronization. The control law is derived from Lyapunov energy function without switching condition. The controller shows robust motion synchronization against disturbances and parameter variations. Proposed SMC control is implemented in conventional double-sided machining operation.

1. Introduction

In order to attain higher productivity and precision at a lower cost, there is a strong demand for developing advanced manufacturing techniques. Various precision motion systems, such as robots and multi-axis computer numerical control (CNC) machine tools require high-speed coordinated motion. As the system traces complex trajectory at high-speed, motion accuracy depends not only on the capability of individual axes that are in motion, but also on their synchronization. A part from the drive based controller design, more robust and coupled control strategies are required to improve the accuracy of complex motion systems. In these applications *"synchronization"* between the drives is favored in parallel to individual set point tracking objective.

A practical example showing the importance of motion synchronization in manufacturing can be observed in the double-sided milling (Mori, Hiramatsu, & Shamoto, 2010; Shamoto, Mori, Nishimura, Hiramatsu, & Kurata, 2010) operation. Double-sided milling has been proposed for finishing thin steel plates to attain improved flatness and surface quality. This process is shown in Fig. 1. In this machining process, thin steel plates are clamped vertically and both sides of the plate are cut simultaneously employing multiple face cutters attached on left and right spindles. The machine tool is presented in Fig. 1a. Dual spindles equipped with cutting tools rotate at high speed and engage with work-piece at identical time instant at each side to remove material. Nonlinear cutting forces are generated acting on the rotational motion of the spindles. Compared to conventional single sided material removal process, this strategy provides higher efficiency and finish accuracy. However, double-sided milling method relies on cutting both sides of the work-piece with precision cutter position synchronization to cancel out process forces in cutting. As a matter of fact, thin work-piece has low structural stiffness in the normal direction due to clamping. A force unbalance will occur if the cutters do not engage with the surface at the same instant. Resultant unbalanced force can trigger forced, or even chatter vibrations (Altintas, 2000) causing thin work-piece to vibrate heavily in normal direction and destroy the surface finish (Mori et al., 2010). This phenomenon is explained in Fig. 2. Therefore, accurate synchronization of teeth positioning, i.e. position synchronization between the right and left spindles, is crucial for achieving high manufacturing quality in this material removal process.

Several approaches have been developed to achieve *"synchronization"* or *"coordination"* in general multi-axis motion systems. A major strategy to introduce coordination between drives is through *'cross coupling controller'*. This method is developed essentially for contouring control of CNC machine tools where contour error or so called the *'path following error'* is calculated in real-time, and a cross coupling controller (CCC) is utilized to inject extra control action to pull the end effector closer to reference

* Corresponding author. Tel.: +81 52 789 4491; fax: +81 52 789 3107.
E-mail addresses: burak@upr.mech.nagoya-u.ac.jp, burak0307@gmail.com (B. Sencer).

0967-0661/$ - see front matter © 2013 Elsevier Ltd. All rights reserved.
http://dx.doi.org/10.1016/j.conengprac.2013.07.001

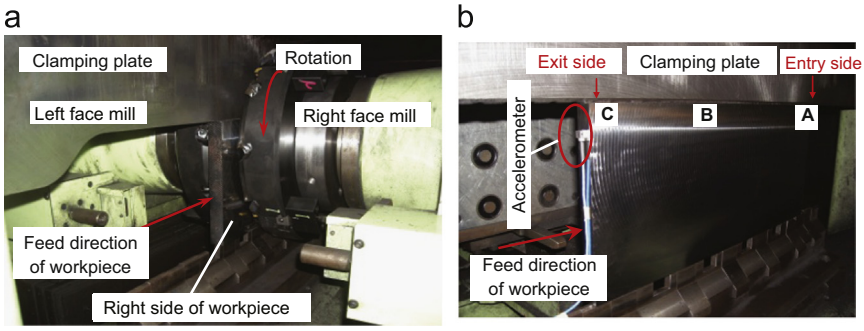

Fig. 1. (a) Double-sided milling machine and process and (b) Work-piece machined by double-sided milling.

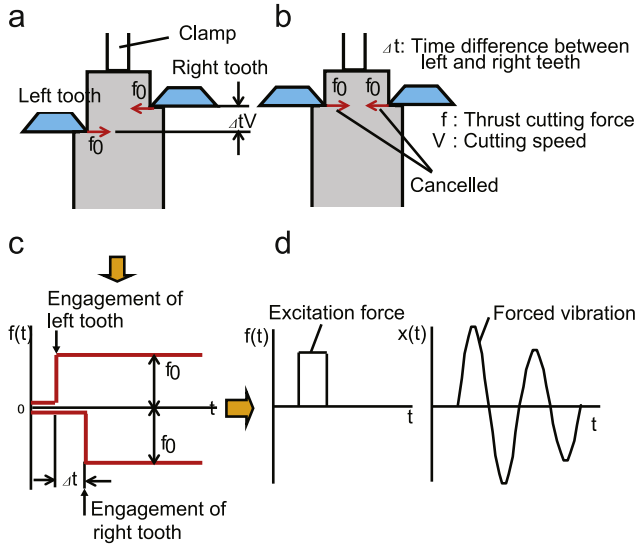

Fig. 2. Importance of motion synchronization for vibration avoidance: (a) With time difference, (b) Without time difference, (c) thrust cutting forces and (d) excitation force and forced vibration.

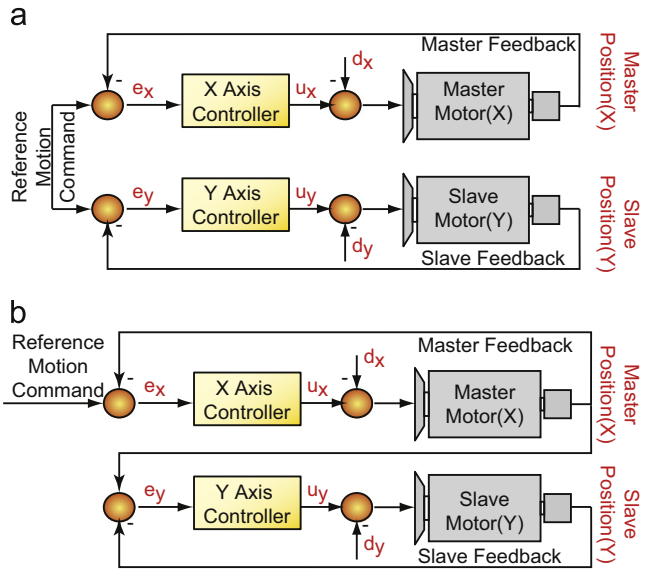

Fig. 3. Control algorithms utilized for motion synchronization: (a) 'Tandem' control, (b) 'Master–slave' control.

path. Koren (1991) founded the CCC and extended it for more complex path following applications (Koren & Lo, 1991). However, the idea of utilizing a contouring controller in conjunction with the existing drive level controller causes controllers to work against each other, and it may jeopardize overall robustness. Furthermore, proving the coupled stability may become cumbersome. Chiu and Tomizuka (2000) tacked this problem by developing a coordinate transformation approach to directly design the controller on contour error dynamics. Peng and Chen (2007) designed a back-stepping sliding mode controller, and later Chen, Liu, and Ting (2007) re-formulated it in polar coordinates. Sencer and Altintas (2009) designed a robust contouring controller for 5-axis CNC machine tools.

In practice, on the other hand, much simpler methods have been favored. For instance, *'master–slave'* control approach has been widely employed and has become a practical "gold standard" for motion synchronization in dual servo drives (Rodriguez-Angeles & Nijmeijer, 2005; Su, Sun., Ren, & Mills, 2006). The master–slave control scheme is shown in Fig. 3b. In this scheme, position of the master motor is used as reference command to the slave, which fundamentally introduces an unavoidable delay between the servos making it practically difficult to achieve perfect synchronization in disturbance sensitive applications.

Another strategy is the indirect or so called the *'tandem control approach'*, shown in Fig. 3a. In this scheme set point tracking errors of drives are minimized using high bandwidth controllers and synchronization in-between is achieved passively through dynamics matching and the reference trajectory generator. Traditional algorithms such as P, PI and PID are based on the feedback principle (Franklin, Powell, & Emami-Naeini, 2009; Su et al., 2006) can be implemented in drive level for precision positioning with vibration suppression (Horowitz, Li, Oldham, Kon, & Huang, 2003; Jinbang, Wenyu, Anwen, & Yu, 2013) capabilities, and servo closed loop dynamics are matched for accurate synchronization (Yeh & Hsu, 2004). Recent efforts are directed towards improving bandwidth and disturbance rejection of the drives using sliding mode controllers that are also robust to changes in drive dynamics. The first servo application of sliding mode controller (SMC) was introduced by Utkin (1977). The original sliding mode controller had required high frequency switching around the sliding surface resulting in a discontinuous control law. It caused control signal chattering and defeated its use in precision servoing. To overcome this, Slotine and Li (1988) proposed adaptive sliding mode controller (ASMC), which estimates and cancels uncertainties that do not necessarily vanish at the equilibrium point. Several countermeasures, such as the use of boundary layer or disturbance observers have been proposed, and guidelines are given in review papers to tackle the control signal chattering problem in SMC design (De Carlo, Zak, & Matthews, 1988; Sabanovic, 2011). One of the main issue lies on the use of discontinuous switching (saturation) function to derive stable sliding mode control law. Resembling a relay controller, sliding mode control laws mostly include a term such as

$$u_{SMC} = u_e + \mathrm{sgn}(\sigma) \tag{1}$$

which forces the control signal polarity to change depending on the location of states around the sliding manifold, σ. Thus, the use of SMC controllers has been limited in precision motion control practice. To address this problem, Altintas, Erkorkmaz, and Zhu (2000) proposed an adaptive sliding mode controller without the switching function and applied it successfully on precision control of ball-screw driven servo systems (Kamalzadeh & Erkorkmaz, 2007). In parallel, robust discrete time sliding mode controls have been designed (Won & Hedrick, 2000). Okwidure (Okwudire & Altintas, 2009) designed a discrete time sliding mode control with mode compensation for vibration suppression and widening the tracking bandwidth of servo systems. He also compared and proved robustness of the sliding mode controller against the industry standard P-PI cascade position control in precision linear motor system (Okwudire. & Altintas, 2008). Recently higher order as well as model reference sliding mode controller has been introduced to eliminate control signal chattering problem and achieve optimal tuning of the sliding mode gains (Muske, Ashrafiuon, Nersesov, & Nikkhah, 2012; Talole & Phadke, 2008). These approaches deliver a chattering-free system, but a finite steady-state error may exist due to imperfect disturbance rejection. Dynamic sliding mode control (Bartolini, Ferrara, & Usai, 1998; Sira-Ramirez, 1993) has been proposed where an integrator is used to eliminate the chattering and at the same time achieve robust disturbance recovery. However, the drawback of dynamic sliding mode control relies in the fact that it requires higher order derivatives of the sliding surface to be known, which in practice may not be measured and requires estimation. Levant (1998) proposed an exact finite time convergence differentiator, which can successfully estimate the derivative of the sliding variable but required a priori bounded trajectory. Later, Khan, Spurgeon, and Levant (2003) proposed a 2-sliding algorithm to stabilize non-linear systems that does not require output derivatives to be measured or observed.

However, widening the tracking bandwidth or just improving the disturbance rejection of a single drive does not necessarily improve synchronization between the drives involved in a coordinated motion. Bottleneck with the axis based approach lies in its passive motion synchronization where disturbances such as un-modeled friction or the cutting forces deteriorate motion coordination that may be detrimental to the process accuracy.

In this research the problem of position synchronization, i.e. motion synchronization, in dual servo drives is addressed. A continuous-time synchronization sliding mode controller is designed to achieve both set-point tracking and robust motion synchronization in dual servo systems. The strategy of the proposed controller is to introduce robust coupling between two drives and penalize synchronization errors that arise due to disturbances, parameter variations as well as un-modeled dynamics within the sliding mode control design scheme. A part from the common literature, proposed controller generates continuous control signal defeating the chattering issue and allows convenient implementation of the SMC in practice. Controller's asymptotic convergence and disturbance adaptation are proven by the Lyapunov function. An industrial application is utilized to prove the effectiveness of the controller.

2. Dual servo drive model

The initial step in designing a robust synchronization sliding mode control is to determine the plant model. In this work higher order structural dynamics of the drives are neglected and simplified rigid body dynamics based model (Levant, 1998) of the servo system is considered. The rigid body model for a single servo drive is presented in Figs. 4 and 5. Neglecting the non-linearities and assuming that there is no physical coupling between the two

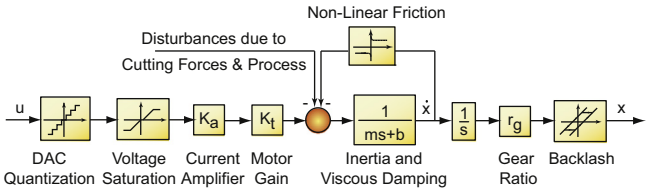

Fig. 4. Rigid body model of an industrial feed drive system.

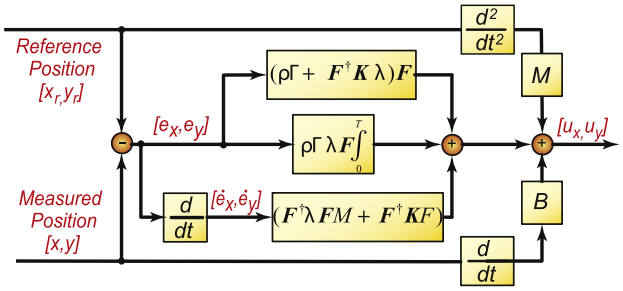

Fig. 5. Block diagram of the proposed sliding mode controller.

drives, the un-coupled dual servo dynamics can be written in matrix form as

$$\underbrace{\begin{bmatrix} u_x \\ u_y \end{bmatrix}}_{u} - \underbrace{\begin{bmatrix} d_x \\ d_y \end{bmatrix}}_{d} = \underbrace{\begin{bmatrix} M_x & 0 \\ 0 & M_y \end{bmatrix}}_{M} \underbrace{\begin{bmatrix} \ddot{x} \\ \ddot{y} \end{bmatrix}}_{\ddot{x}} + \underbrace{\begin{bmatrix} B_x & 0 \\ 0 & B_y \end{bmatrix}}_{B} \underbrace{\begin{bmatrix} \dot{x} \\ \dot{y} \end{bmatrix}}_{\dot{x}} \tag{2}$$

The model considers that amplifiers run in the torque control mode where u [V] is the control equivalent torque command delivered, and d [V] is the external disturbances reflected at the control signal input. $\mathbf{M} = diag(M_x, M_y)$ and $\mathbf{B} = diag(B_x, B_y)$ are diagonal matrices that contain drives' equivalent inertia $M_x = m/K_aK_tr_g$ and viscous friction $B_x = b/K_aK_tr_g$ terms normalized by the amplifier K_a and motor torque constants K_t as well as the gear ratio, r_g. $\mathbf{x} = [x, y]^T, \dot{\mathbf{x}} = [\dot{x}, \dot{y}]^T, \ddot{\mathbf{x}} = [\ddot{x}, \ddot{y}]^T$ presents drive's actual position, velocity and acceleration kinematics. It should be noted that although the model is based on linear dynamics of the servo system, several non-linearities such as the friction, backlash, amplifier saturation as well as cutting disturbances affect the controller performance (Mori et al., 2010; Okwudire & Altintas, 2008). Particularly, in real industrial applications effect of those parameters becomes significant in precision motion synchronization. Introducing the reference motion trajectory, $\mathbf{x}_{ref} = [x_{ref}, y_{ref}]$, tracking error dynamics can be written from Eq. (2) as

$$\ddot{\mathbf{e}} = \begin{bmatrix} \ddot{e}_x \\ \ddot{e}_y \end{bmatrix} = \ddot{\mathbf{x}}_{\mathbf{ref}} - \mathbf{M}^{-1}(\mathbf{u} - \mathbf{d} - \mathbf{B}\dot{\mathbf{x}}) \tag{3}$$

The objective of the proposed controller is to satisfy accurate set-point tracking and at the same time actively minimize the synchronization errors between two servo drives that occur due to cutting disturbances and un-modeled dynamics. A *synchronization error* state is defined as the differential position error between the two servo drives, such as the X and Y as

$$\varepsilon = e_x - e_y \tag{4}$$

where $e_x = x_{ref} - x$ is set-point tracking error of X-axis and $e_y = y_{ref} - y$ is for the Y-axis, respectively. Synchronization errors (ε) between two drives can be calculated from individual tracking errors using the following transformation:

$$\begin{bmatrix} e_x \\ e_y \\ \varepsilon \end{bmatrix} = \underbrace{\begin{bmatrix} 1 & 0 \\ 0 & 1 \\ 1 & -1 \end{bmatrix}}_{F} \underbrace{\begin{bmatrix} e_x \\ e_y \end{bmatrix}}_{\mathbf{e}} \tag{5}$$

where $F_{3\times 2}$ is a transformation matrix. Augmented with the synchronization error state, error dynamics for the dual servo system can be computed from Eqs. (3) and (5) as

$$\begin{bmatrix}\dot{e}_x\\ \dot{e}_y\\ \dot{\varepsilon}\end{bmatrix}=\mathbf{F}\dot{\mathbf{e}} \text{ and } \begin{bmatrix}\ddot{e}_x\\ \ddot{e}_y\\ \ddot{\varepsilon}\end{bmatrix}=\mathbf{F}\ddot{\mathbf{x}}_{\mathbf{ref}}-\mathbf{F}\mathbf{M}^{-1}(\mathbf{u}-\mathbf{d}-\mathbf{B}\dot{\mathbf{x}}). \tag{6}$$

3. Synchronization sliding mode controller design

The overall objective of the controller is to minimize all the 3 error states presented in Eq. (5), namely the individual drive tracking errors and the synchronization errors in the dual servo system.

First step of designing a SMC is to select a stable sliding surface. In order to penalize both, the tracking and synchronization errors, a 3 dimensional 1st order sliding surface ($\boldsymbol{S}$) is defined as

$$\mathbf{S}_{3\times 1}=\begin{bmatrix}S_x\\ S_y\\ S_z\end{bmatrix}=\lambda_{3\times 3}\mathbf{F}_{3\times 2}\mathbf{e}_{2\times 1}+\mathbf{F}_{3\times 2}\dot{\mathbf{e}}_{2\times 1}. \tag{7}$$

$\lambda=diag(\lambda_x,\lambda_y,\lambda_\varepsilon)$ is the sliding surface parameter, which defines the convergence speed of the errors on the sliding surface. Owing the nature of sliding mode controllers, there is a plant inversion inhered to cancel the open loop dynamics. However, due to modeling errors of the servo system, and external disturbances such as the process forces, error states are pulled away from the sliding manifold. In order to ensure zero steady state errors and introduce robustness to the controller, the following disturbance observer $\hat{\mathbf{d}}$ is defined, which penalizes deviation of errors from the sliding manifold by integrating the sliding surface based on Eq. (7) as

$$\dot{\hat{\mathbf{d}}}=\begin{bmatrix}\dot{\hat{d}}_x\\ \dot{\hat{d}}_y\end{bmatrix}=\rho\kappa\Gamma\dot{\mathbf{S}} \quad\rightarrow\quad \hat{\mathbf{d}}=\begin{bmatrix}\hat{d}_x\\ \hat{d}_y\end{bmatrix}=\rho\kappa\Gamma\int(\lambda\mathbf{F}\mathbf{e}+\mathbf{F}\dot{\mathbf{e}})d\tau. \tag{8}$$

As shown in Eq. (8), postulated observer integrates the sliding surface to penalize deviation of error dynamics from the surface. $\rho=diag(\rho_x,\rho_y)$ is the diagonal positive definite observer gain matrix. In the implementation, it becomes a tuning variable for the sliding mode controller. It should be noted that integration is performed only on the drive level by the use of the following transformation matrix:

$$\Gamma=\begin{bmatrix}1 & 0 & 0\\ 0 & 1 & 0\end{bmatrix} \tag{9}$$

so that the sliding surface is integrated in the S_x and S_y directions excluding the synchronization dynamics, S_ε. This allows the controller to introduce higher static stiffness on the drive level and provide robustness against disturbances. More importantly, it eliminates the illusion that synchronization errors may converge to zero even if the tracking errors are non-zero. By imposing the disturbance observer only in the drive level controller makes sure that steady state tracking errors are strictly diminished. Diagonal $\kappa=diag(\kappa_x,\kappa_y)$ is defined to impose bounds on the observed disturbances so that the adaptations, i.e. integrations, are kept within the predetermined bounds $\hat{d}_x^-\le\hat{d}_x\le\hat{d}_x^+$ and $\hat{d}_y^-\le\hat{d}_y\le\hat{d}_y^+$. This resembles a conventional integral anti-wind-up function. For instance, κ_x is defined for $\hat{d}_x$ is written as

$$\kappa_x=\begin{Bmatrix}0 & \text{if } \hat{d}_x\le d_x^- \text{ and } S_x\le 0\\ 0 & \text{if } \hat{d}_x\ge d_x^- \text{ and } S_x\ge 0\\ 1 & \text{otherwise}\end{Bmatrix}. \tag{10}$$

and similar for $\hat{d}_y$ it becomes

$$\kappa_y=\begin{Bmatrix}0 & \text{if } \hat{d}_y\le d_y^- \text{ and } S_y\le 0\\ 0 & \text{if } \hat{d}_y\ge d_y^- \text{ and } S_y\ge 0\\ 1 & \text{otherwise}\end{Bmatrix}. \tag{11}$$

It should be noted that although $\kappa_{2\times 2}$ could be interpreted as time variant, it functions as a switching operator that only becomes active in case if the adaptation for external disturbances exceed the predetermined bounds and the error states are not on a convergent trajectory to the sliding manifold. The observer bounds $\hat{d}\in[\hat{d}^+,\hat{d}^-]$ can be selected as the saturation limits of servo amplifiers to ensure robust operation.

The following energy-like Lyapunov function:

$$E=\tfrac{1}{2}\left[\mathbf{S}^T\mathbf{S}+(\mathbf{d}-\hat{\mathbf{d}})^T(\mathbf{M}\rho)^{-1}(\mathbf{d}-\hat{\mathbf{d}})\right] \tag{12}$$

is postulated to derive a stable SMC control law for the dual feed drive system synchronized by the proposed strategy. As shown in Eq. (12), E penalizes the total energy of the system, first depending on the discrepancy of the errors from the sliding surface dynamics by the $\mathbf{S}^T\mathbf{S}$ term, and second, the disturbance adaptation errors by the $(\mathbf{d}-\hat{\mathbf{d}})^T(\mathbf{M}\rho)^{-1}(\mathbf{d}-\hat{\mathbf{d}})$ term. In order to generate a stable sliding mode control law, derivative of the Lyapunov function ($\dot{E}$) must be negative. This ensures that the energy will decrease, errors states will be pulled onto the sliding manifold, and adaptation law will converge for slowly varying disturbances. As a result, asymptotic stability of the overall system could be achieved. Derivative of the Lyapunov energy function is computed from Eq. (12) as

$$\begin{aligned}\dot{E}&=\frac{1}{2}\left[\dot{\mathbf{S}}^{\mathbf{T}}\mathbf{S}+\mathbf{S}^T\dot{\mathbf{S}}+(\dot{\mathbf{d}}-\dot{\hat{\mathbf{d}}})^{\mathbf{T}}(\mathbf{M}\rho)^{-1}(\mathbf{d}-\hat{\mathbf{d}})+(\mathbf{d}-\hat{\mathbf{d}})^{\mathbf{T}}(\mathbf{M}\rho)^{-1}(\dot{\mathbf{d}}-\dot{\hat{\mathbf{d}}})\right]\\ &=\mathbf{S}^T\dot{\mathbf{S}}-(\mathbf{d}-\hat{\mathbf{d}})^{\mathbf{T}}(\mathbf{M}\rho)^{-1}\dot{\hat{\mathbf{d}}}\end{aligned} \tag{13}$$

It should be noted that since only slowly changing disturbances are adapted for, derivative of the actual disturbances is considered to be zero, $\dot{\mathbf{d}}=0$. Eq. (13) is further expanded by substituting derivative of the sliding surface from Eqs. (6) and (7) as

$$\begin{aligned}\dot{E}&=\mathbf{S}^T[\lambda\mathbf{F}M\dot{\mathbf{e}}+\mathbf{F}M\ddot{\mathbf{x}}_{\mathbf{ref}}-\mathbf{F}(\mathbf{u}-d-\mathbf{B}\dot{\mathbf{x}})]-(\mathbf{d}-\hat{\mathbf{d}})^{\mathbf{T}}(\rho)^{-1}\dot{\hat{\mathbf{d}}}\\ &=\mathbf{S}^{\mathbf{T}}[\lambda\mathbf{F}M\dot{\mathbf{e}}+\mathbf{F}M\ddot{\mathbf{x}}_{\mathbf{ref}}-\mathbf{F}(\mathbf{u}-\mathbf{B}\dot{\mathbf{x}})]+\mathbf{S}^{\mathbf{T}}\mathbf{F}\mathbf{d}-(\mathbf{d}-\hat{\mathbf{d}})^{\mathbf{T}}(\rho)^{-1}\dot{\hat{\mathbf{d}}}.\end{aligned} \tag{14}$$

and substituting the disturbance observer expression from Eq. (8) leads to

$$\dot{E}=\mathbf{S}^{\mathbf{T}}[\lambda\mathbf{F}M\dot{\mathbf{e}}+\mathbf{F}M\ddot{\mathbf{x}}_{\mathbf{ref}}-\mathbf{F}(\mathbf{u}-\mathbf{B}\dot{\mathbf{x}})]+\mathbf{S}^{\mathbf{T}}\mathbf{F}\mathbf{d}-\mathbf{S}^{\mathbf{T}}\Gamma^T\kappa(\mathbf{d}-\hat{\mathbf{d}}) \tag{15}$$

Eq. (15) is re-written by adding and subtracting $\mathbf{S}^{\mathbf{T}}\mathbf{F}^{\mathbf{T}}\hat{\mathbf{d}}$,

$$\begin{aligned}\dot{E}=&\mathbf{S}^{\mathbf{T}}[\lambda\mathbf{F}M\dot{\mathbf{e}}+\mathbf{F}M\ddot{\mathbf{x}}_{\mathbf{ref}}-\mathbf{F}(\mathbf{u}-\mathbf{B}\dot{\mathbf{x}})]\\ &+\underbrace{\mathbf{S}^{\mathbf{T}}\mathbf{F}\mathbf{d}+\mathbf{S}^{\mathbf{T}}\mathbf{F}\hat{\mathbf{d}}-\mathbf{S}^{\mathbf{T}}\mathbf{F}\hat{\mathbf{d}}-\mathbf{S}^{\mathbf{T}}\Gamma^T\kappa(\mathbf{d}-\hat{\mathbf{d}})}_{\mathbf{S}^{\mathbf{T}}\mathbf{F}\hat{\mathbf{d}}+\mathbf{S}^{\mathbf{T}}(\mathbf{F}-\Gamma^T\kappa)(\mathbf{d}-\hat{\mathbf{d}})}\end{aligned} \tag{16}$$

where the final terms can be grouped as $\mathbf{S}^T\mathbf{F}\hat{\mathbf{d}}+\mathbf{S}^T(\mathbf{F}-\Gamma^T\kappa)(\mathbf{d}-\hat{\mathbf{d}})$, and due to the disturbance observer bounds imposed in Eqs. (10) and (11), $\mathbf{S}^T(\mathbf{F}-\Gamma^T\kappa)(\mathbf{d}-\hat{\mathbf{d}})\le\mathbf{0}$ can be observed. Thus, if remaining terms in the Lyapunov derivative (Eq. (16)) could be forced to be negative definite, stable control law can be derived. The key is to select an appropriate forcing function to generate a continuous sliding mode control law. Unlike the conventional sliding mode control where *sgn* or *sat* function is simply employed for forcing derivative of the Lyapunov to be negative, which may generate discontinuous control law (Slotine & Li, 1988), the following condition is postulated for achieving asymptotic stability ($\dot{E}(t)<0$):

$$\dot{E}=\mathbf{S}^{\mathbf{T}}[\lambda\mathbf{F}\mathbf{M}\dot{\mathbf{e}}+\mathbf{F}\mathbf{M}\ddot{\mathbf{x}}_{\mathbf{ref}}-\mathbf{F}(\mathbf{u}-\mathbf{B}\dot{\mathbf{x}})]+\mathbf{S}^{\mathbf{T}}\mathbf{F}\hat{\mathbf{d}}=-\mathbf{S}^{\mathbf{T}}\mathbf{K}\mathbf{S}. \tag{17}$$

where $\mathbf{K}_{3\times 3}=diag(K_x,K_y,K_\varepsilon)$contains positive definitive feedback gains, and the control command is extracted from Eq. (17) as

$$\lambda\mathbf{F}\mathbf{M}\dot{\mathbf{e}}+\mathbf{F}\mathbf{M}\ddot{\mathbf{x}}_{\mathbf{ref}}+\mathbf{F}\mathbf{B}\dot{\mathbf{x}}+\mathbf{F}\hat{\mathbf{d}}+\mathbf{K}\mathbf{S}=\mathbf{F}\mathbf{u}. \tag{18}$$

Substituting disturbance observer from Eq. (8) and the sliding surface $\mathbf{S}=\lambda\mathbf{Fe}+\mathbf{F}\dot{\mathbf{e}}$, into Eq. (18) leads to the following control law:

$$\mathbf{M}\ddot{\mathbf{x}}_{\mathbf{ref}}+\mathbf{B}\dot{\mathbf{x}}+\mathbf{F}^{\dagger}\lambda\mathbf{F}\mathbf{M}\dot{\mathbf{e}}+\mathbf{F}^{\dagger}\mathbf{K}\lambda\mathbf{F}\mathbf{e}+\mathbf{F}^{\dagger}\mathbf{K}\mathbf{F}\dot{\mathbf{e}}+\rho\kappa\Gamma\int\mathbf{S}\mathrm{d}\tau=\mathbf{u}. \tag{19}$$

It should be noted that $\mathbf{F}^{\dagger}$ is the pseudo-inverse of $\mathbf{F}$. At last, assuming that the system works in the linear region or setting the observer bounds ($\hat{d}_{x,y}^{\pm}$) large enough e.g. drive's saturation limits, allows omitting the adaptation bound matrix(κ). Grouping the terms leads to the final control law:

$$[\mathbf{M}\ddot{\mathbf{x}}_{\mathbf{ref}}+\mathbf{B}\dot{\mathbf{x}}]+(\rho\Gamma+\mathbf{F}^{\dagger}\mathbf{K}\lambda)\mathbf{F}\mathbf{e}+\rho\Gamma\lambda\mathbf{F}\int\mathbf{e}\mathrm{d}\tau+(\mathbf{F}^{\dagger}\lambda\mathbf{F}\mathbf{M}+\mathbf{F}^{\dagger}\mathbf{K}\mathbf{F})\dot{\mathbf{e}}=\mathbf{u}, \tag{20}$$

which does not contain any switching function. Further proof on the error convergence is presented in Appendix section.

4. Controller analysis

This section presents insight on the proposed synchronization sliding mode controller and gives guidelines for proper tuning for control engineer's practice. By inspecting the terms in the proposed synchronization SMC law (Eq. (20)), particular gains can be grouped as follows:

$$(\mathbf{M}\ddot{\mathbf{x}}_{\mathbf{ref}}+\mathbf{B}\dot{\mathbf{x}})+\underbrace{(\rho\Gamma+\mathbf{F}^{\dagger}\mathbf{K}\lambda)\mathbf{F}\mathbf{e}}_{\text{ProportionalGain}}+\underbrace{\rho\Gamma\lambda\mathbf{F}\int\mathbf{e}\mathrm{d}\tau}_{\text{IntegralGain}}+\underbrace{(\mathbf{F}^{\dagger}\lambda\mathbf{F}\mathbf{M}+\mathbf{F}^{\dagger}\mathbf{K}\mathbf{F})\dot{\mathbf{e}}}_{\text{DerivativeGain}}=\mathbf{u}. \tag{21}$$

The continuous control law resembles a PID structure with 4 main terms. The 1st term presents feed-forward mass compensation to widen the tracking bandwidth and additional damping. The last 3 terms can be interpreted as multivariable PID gains that present proportional, derivative and the integral action matrices mapped from the sliding mode controller's gains. Guidelines for tuning the proposed controller's gains are summarized as

- $\lambda=diag(\lambda_x,\lambda_y,\lambda_\varepsilon)$ dictate desired bandwidth for tracking. If individual X and Y servo drive dynamics do not differ dramatically, tracking bandwidths λ_x and λ_y can be set identical to achieve the same error decay. Synchronization bandwidth term λ_ε determines the coupling action in low and mid frequency range of control bandwidth. As a guideline λ_ε should be selected higher than the axial parameters, $\lambda_\varepsilon=5$–$50\lambda_{x,y}$.
- $\mathbf{K}=diag(K_x,K_y,K_\varepsilon)$is SMC feedback gains. It determines how much control action is produced to penalize deviation of error states from sliding surface. Increasing K_ε will essentially introduce synchronization effect at higher frequencies and should not be set much higher than the axis level, e.g. $K_\varepsilon=1$–$3K_{x,y}$ to eliminate excess noise entering the system.
- The final parameter set contains the disturbance observer gains, $\rho=diag(\rho_x,\rho_y)$ to eliminate steady state tracking errors while adding stiffness to the system.

Neglecting the feed-forward terms, proposed synchronization SMC control law can also be implemented as a multi-input multi-output (MIMO) PID controller with the following compensator matrix:

$$\mathbf{C}(s)=\begin{bmatrix}\underbrace{\mathbf{K}p_{xx}+\mathbf{K}d_{xx}s+\mathbf{K}i_{xx}\frac{1}{s}}_{\mathbf{c}_{xx}} & \underbrace{\mathbf{K}p_{xy}+\mathbf{K}d_{xy}s}_{\mathbf{c}_{xy}}\\ \underbrace{\mathbf{K}p_{yx}+\mathbf{K}d_{yx}s}_{\mathbf{c}_{yx}} & \underbrace{\mathbf{K}p_{yy}+\mathbf{K}d_{yy}s+\mathbf{K}i_{yy}\frac{1}{s}}_{\mathbf{c}_{yy}}\end{bmatrix}. \tag{22}$$

where K_p, K_i, K_d matrices are computed from Eq. (21). Re-writing the closed loop dynamics using Eqs. (3) and (22) results in

$$\underbrace{\begin{bmatrix}G_x(s) & 0\\ 0 & G_y(s)\end{bmatrix}}_{\mathbf{G}(s)}\underbrace{\begin{bmatrix}C_{xx}(s) & C_{xy}(s)\\ C_{yx}(s) & C_{yy}(s)\end{bmatrix}}_{\mathbf{C}(s)}\begin{bmatrix}e_x\\ e_y\end{bmatrix}-\underbrace{\begin{bmatrix}G_x(s) & 0\\ 0 & G_y(s)\end{bmatrix}}_{\mathbf{G}(s)}\begin{bmatrix}d_x\\ d_y\end{bmatrix}=\begin{bmatrix}x_{ref}-e_x\\ y_{ref}-e_y\end{bmatrix}. \tag{23}$$

where $\mathbf{G}(s)$ contains plant dynamics such as $G_x(s)=1/(M_xs^2+B_xs)$ and $G_y(s)=1/(M_ys^2+B_ys)$. Further expansion of Eq. (23) results in the coupled error dynamics:

$$e_x=\frac{x_{ref}+d_xG_x-C_{xy}G_xe_y}{1+C_{xx}G_x},\quad e_y=\frac{y_{ref}+d_yG_y-C_{yx}G_ye_x}{1+C_{yy}G_y}. \tag{24}$$

Assuming that the plant dynamics are identical as well as the controller gains are matched for a servo system $G_p=G_x\cong G_y$, $C_c=C_{xx}\cong C_{yy}$ and $C_{xy}\cong C_{yx}$, Eq. (24) can be simplified to calculate the transfer function governing synchronization error dynamics as

$$\varepsilon=\frac{(x_{ref}-y_{ref})+G_p(d_x-d_y)}{C_cG_p+1-C_{xy}G_p}. \tag{25}$$

For synchronized motion tracking, the reference trajectory commanded to the drives is also identical $x_{ref}=y_{ref}$, which results in

$$\varepsilon=\frac{(d_x-d_y)}{C_c+1/G_p-C_{xy}}. \tag{26}$$

Eq. (26) reveals that synchronization errors are governed by the unmatched disturbances d_x-d_y in a dynamically matched servo system. In contrast to a conventional tandem PID controlled servo system, proposed synchronization SMC control introduces negative cross term C_{xy} to robustly introduce synchronization and coupling between the dual servos against disturbances. Therefore, it reveals that proposed controller achieves both set-point tracking and at the same time motion synchronization. Contrarily, when the disturbances are identical $d_x-d_y=0$, synchronization errors would be $\varepsilon=0$. It can be noted that in this case cross terms do not affect the controller performance, and the tracking dynamics of the servo system is not altered.

5. Experimental results

Depending on the application, objective of the controller is mainly to improve the synchronization performance of a dual motor servo system against disturbances and un-modeled dynamics. Controller performance is first experimentally tested on a dual linear motor slider setup where uneven external disturbances are injected to the system to disturb synchronization, and a MIMO analysis is presented to give an insight on the parameter tuning. Finally, proposed controller is implemented on a commercial double-sided milling machine tool (Mori et al., 2010) where controller performance is validated in real manufacturing operation against conventional as well as robust servo control schemes.

5.1. Experimental implementation and MIMO analysis

The experimental dual motor test platform for controller implementation is shown in Fig. 6. In this setup two identical blushless Permanent Magnet (PM) linear motors, Motor X and Motor Y, are driving carts simulating a synchronized assembly line. Linear motors are driven separately by identical amplifiers that run in torque, i.e. current control mode, and the Dspace 1103 DSP (Digital Signal Processing) system is used for real time control.

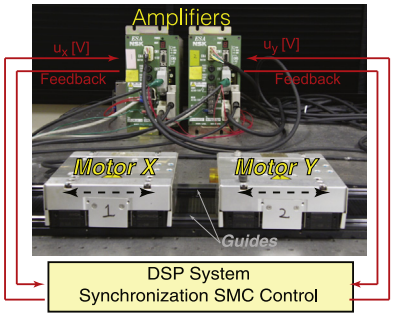

Fig. 6. Permanent magnet dual linear motor setup.

Table 1
Rigid body parameters of the dual linear motor system.

Motor	Equivalent mass (Volts/mm/s^2) $M=m/K_aK_tr_g$	Equivalent friction (Volts/mm/s) $B=b/K_aK_tr_g$	Encoder resolution (counts/mm)	Coulomb friction (Volts)
Motor X	0.25536×10^{-3}	0.76467×10^{-3}	4000	T_{pos}=0.15725 T_{neg}=0.14677
Motor Y	0.26006×10^{-3}	0.89919×10^{-3}	4000	T_{pos}=0.23367 T_{neg}=0.18512

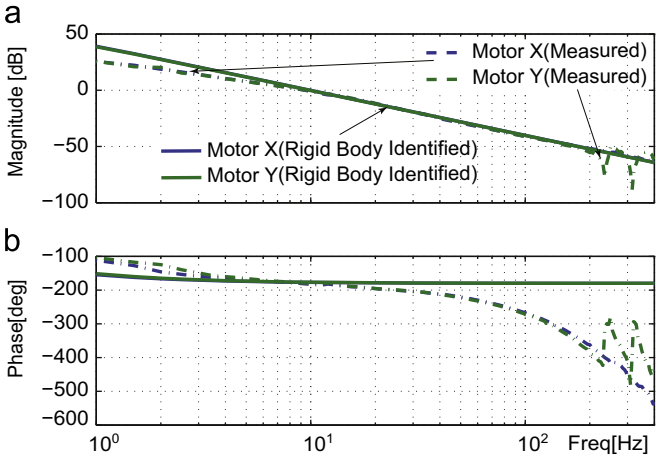

Fig. 7. Open loop frequency response of the dual linear motor setup: (a) open loop amplitude and (b) open loop phase.

Encoder feedback is taken from the motor side and the torque command $u_{x,y}$ is delivered to amplifiers directly. The controller is simply discretized using backward differentiation. In fact, more exact methods can also be employed (Franklin et al., 2009). The real time control system is set to run at 1 kHz closed loop sampling.

Motor masses M and viscous friction B parameters are identified from time domain identification method (Erkorkmaz & Altintas, 2001), and presented in Table 1. Open loop frequency response for both drives, $G_x(j\omega)$ and $G_y(j\omega)$, are given in Fig. 7. As observed, open loop frequency responses of the drives are almost identical except some high frequency fluctuations due to amplifier noise, torque ripples and resolution of the resolver. Identified rigid body model parameters match the frequency response measurements apart from the effect of coulomb friction in low frequency range, and amplifier delay is dominant at high frequency region. Those discrepancies are considered to be internal disturbance, and they are ought to be compensated by the controller.

MIMO analysis is performed to give an insight on the performance of proposed controller for 5 different parameter sets. Tested

Table 2
Parameter set of the controller.

Controller parameter set	Base gains	Synchronization sliding surface gain (λ_ε)	Synchronization feedback gain (K_ε)
1	$\lambda_x=1,\lambda_y=1$	1	1
2	$K_x=0.02,K_y=0.02$	25	1
3	$\rho_x=1,\rho_y=1$	50	1
4	$\hat{d}^{\pm}_{x,y}=\pm10$	1	3
5		1	

controller parameters are given in Table 2 where both synchronization gains λ_ε and K_ε are increased gradually. The observer saturation bounds are matched with the amplifiers' torque limits, $\hat{d}^{\pm}_{x,y}=\pm10$ V. Results are summarized in Fig. 8. Fig. 8a presents singular values of the multivariable loop transfer matrix $\mathbf{L}(j\omega)=\mathbf{G}(j\omega)\mathbf{C}(j\omega)$ indicating combined amplification of controller and the plant. In Fig. 8a, solid lines present maximum singular value $\overline{\sigma}=\max\{\Sigma_{L(j\omega)}\}$ and dashed lines show the minimum singular value $\underline{\sigma}=\min\{\Sigma_{L(j\omega)}\}$ of the loop transfer matrix as controller gains are altered. As shown, for the initial parameter set, $\lambda_x=\lambda_y=\lambda_\varepsilon=1$, and $K_x=K_y=K_\varepsilon=1$, there is no coupling between the drives, thus maximum and minimum singular values are identical. As the synchronization gain, λ_ε is increased, maximum amplification is increased gradually around all frequencies. In contrast, when K_ε is increased, its effect can be observed especially around higher frequencies. MIMO sensitivity function is defined as $\mathbf{S}(j\omega)=(\mathbf{I}_{2\times2}+\mathbf{L}(j\omega))^{-1}$, and the maximum singular value of sensitivity $\max_{\omega}\sigma\{\Sigma_{S(j\omega)}\}$ is presented in Fig. 8b. It can be observed that increase in the sensitivity is caused mainly by K_ε, which in return reduces the stability margins. In contrast, increasing λ_ε does not affect the sensitivity unfavorably by just causing a slight increase and still improving synchronization robustly. Singular values of disturbance transfer function $\mathbf{D}(j\omega)=\mathbf{S}(j\omega)\mathbf{G}(j\omega)$ are shown in Fig. 8c. Difference between maximum and minimum singular value of the disturbance transfer function can be observed easily. This indicates coupling action imposed by the controller. Physically, the difference between maximum and minimum singular values can be interpreted as follows. From maximum singular value, it can be noted that if the disturbances acting on the motors are in the same direction, i.e. synchronization is not affected directly; overall system shows a more compliant response. Minimum singular value, on the other hand, indicates that if disturbances act in reverse directions, synchronization is deteriorated severely, and the system becomes less compliant showing stronger resistance against external forces. This can also be seen by computing the interaction value of the transmission matrix, which considers the ratio between cross and diagonal terms:

$$\text{Interaction value}(j\omega)=\text{cross}(\mathbf{L}(j\omega))\cdot\text{diag}(\mathbf{L}(j\omega)). \quad (27)$$

Fig. 8d shows the interaction value. Observed from previous parameters, increase in the synchronization gain λ_ε introduces coupling at lower frequency spectrum and at a wider range. In contrast, increasing K_ε introduces stronger synchronization mostly around a higher frequency range. Stability of the controller can simply be tested from MIMO Nyquist criteria. As shown in Fig. 8e, determinant of the multivariable loop transmission matrix $\det(\mathbf{I}_{2\times2}+\mathbf{L}(j\omega))$ does not show any counter-clockwise encirclement around the origin, or it does not cross the origin indicating that the control system is stable for all the given parameter sets.

Tracking experiments are performed on the linear motor setup for validating the performance of the proposed controller for the parameter set given in Table 2. In order to disturb the synchronization of the motors, a 10 kg payload mass is placed on the Motor X, which roughly doubles its inertia ($\overline{M}_x=0.000482\ V/\text{mm}/s^2$)

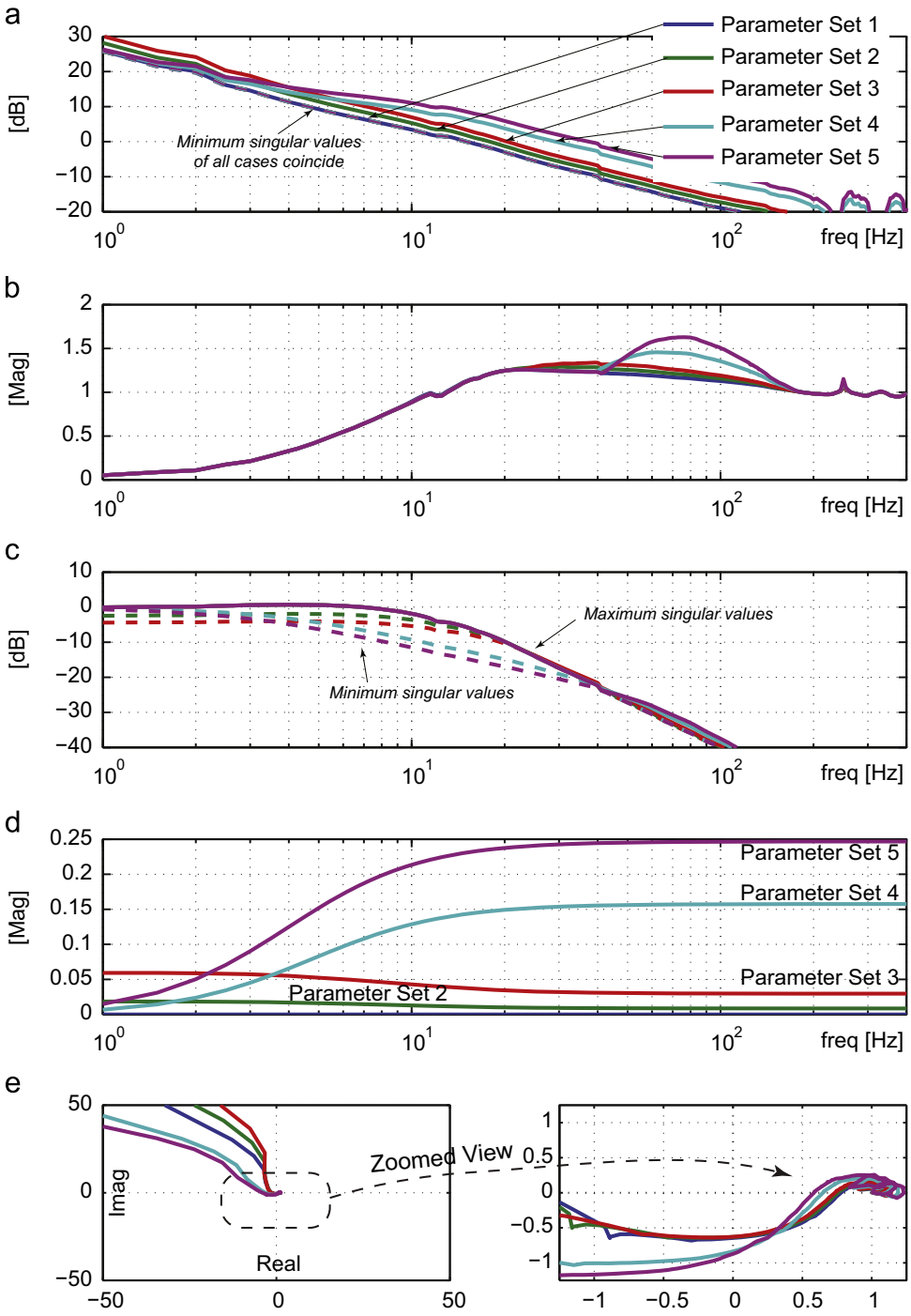

Fig. 8. MIMO analysis of the control system: (a) singular values of the loop transfer matrix, (b) maximum singular value of sensitivity matrix, (c) singular values of disturbance transfer matrix, (d) interaction value of the loop transfer matrix, and (e) multivariable Nyquist plot.

from the original value (see Table 1), and identical back-and-forth motion trajectories with jerk-limited trapezoidal acceleration profile shown in Fig. 9 are commanded to both motors. As noted, due to the added mass, reference trajectory provides a natural disturbance against motion synchronization during acceleration sections. Results of tracking tests are summarized in Fig. 10.

Fig. 10a and b presents tracking errors of the drives for the given set of controller parameters. Motor X shows tracking errors mostly correlated with the acceleration profile of the reference trajectory (see Fig. 9) and roughly 2 times that of the Motor Y. It is also noticeable that as λ_ε is increased from 1 to 50, tracking errors of Motor X decrease gradually, and for Motor Y, in contrast, there is a correlated rise. Gradient of this change is higher as compared to increasing only K_ε. This can be attributed to the fact that λ_ε has more significant effect at lower frequency on the synchronization performance (see Fig. 8). Furthermore, dominant frequency content of a jerk-limited trajectory is generally below 20–30 Hz and thus, disturbances induced by the added mass would affect synchronization errors accordingly in low frequency range. Motor Y tracking errors show some trajectory un-correlated and transient components since the controller commands the lighter Motor Y to assist the heavier axis while still tracking the reference motion trajectory. Experimentally recorded synchronization errors are also presented in Fig. 10c. Summarized in Fig. 11, increasing λ_ε

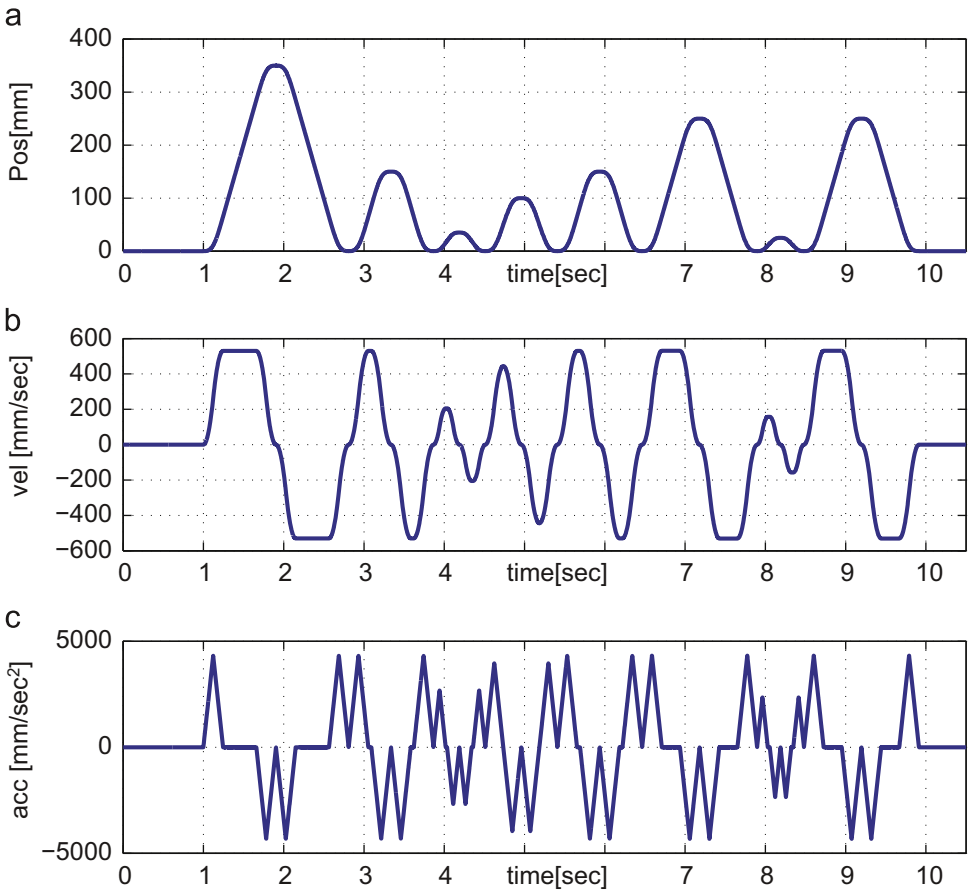

Fig. 9. Reference motion trajectory: (a) reference position profile, (b) reference velocity profile and (c) reference acceleration profile.

improves the synchronization more directly, and maximum as well as the RMS of synchronization errors is reduced around ~50% in this setup. This shows the effectiveness of the sliding mode controller for achieving robust synchronization performance.

At last, average of the tracking errors of Motor X and Y

$$e_{COG} = x_r - \frac{x+y}{2} = \frac{e_x + e_y}{2}, \tag{28}$$

or so called the 'center of motion errors' (known as the 'center of gravity' (COG) errors in practice) is plotted in Fig. 10d. It can be interpreted that the center of gravity response governed by the least amplified direction of the controller and determined by the minimum singular value of the loop transfer matrix. During the tracking experiments, COG errors do not show significant change by the increase agreeing with the MIMO analysis presented above. Especially, during acceleration segments where driving force is utilized heavily, maximum COG errors are identical for all the parameter sets validating that the proposed controller does not jeopardize overall tracking performance.

5.2. Industrial implementation and validation

The proposed control algorithm is implemented and tested in a conventional manufacturing system, which demands not only set point tracking but also synchronization performance. Double-sided milling process was introduced in Fig. 1. This process is based on cutting both sides of a thin work-piece with cutters mounted on identical left and right spindles, Spindle X and Spindle Y, where they are desired to enter the material at the same instant. Cutting forces disturb the synchronization between the left and right cutters as they engage and disengage the material. In order to ensure moderate synchronization, *master–slave* control approach has already been utilized in this conventional milling machine as depicted in Fig. 12a. Proposed sliding mode controller is compared against 2 controllers. First, it is compared against the industrial standard *master–slave* approach where both drives are equipped with P-PI (Franklin et al., 2009) controllers. The *master–slave* controller is tuned by the commercial manufacturer of the control system. It should be noted that due to the black box structure of the commercial servo manufacturer, controller gains could not be determined accurately. However, synchronization errors and torque signals could be logged from the amplifier's analog monitor channels. Second, a continuous time adaptive sliding mode controller (ASMC) given in (Kamalzadeh & Erkorkmaz, 2007) is implemented to benchmark the proposed sliding mode controller. In order to implement the controllers, conventional *master–slave* control is canceled by switching amplifiers of the CNC into torque mode, modifying the PLC, and the dSpace system was used for closed loop real-time control at 1 kHz. Reflected rigid body plant dynamics are identified for the X and Y spindles to be, $B_x = 3.9813 \times 10^{-4}\ V/\mathrm{rad}/s$, $J_x = 3.7337 \times 10^{-4}\ V/\mathrm{rad}/s^2$ and $B_y = 4.3592 \times 10^{-4}\ V/\mathrm{rad}/s$, $J_y = 3.4301 \times 10^{-4}\ V/\mathrm{rad}/s^2$ showing close agreement in the inertia and slight difference in viscous friction. Proposed controller's gains are simply determined based on the above rigid body model and the MIMO analysis. Thereafter, fine-tuning is performed in the implementation on the double-sided milling CNC machine tool to accommodate for the un-modeled drive and process dynamics as well as the noise. The proposed controller's gains are set to $\lambda_{x,y} = 5, \lambda_\varepsilon = 20, \rho_{x,y} = 2, K_{x,y} = 1, K_\varepsilon = 1, \hat{d}^{\pm}_{x,y} = \pm 10$. The benchmark ASMC (Kamalzadeh & Erkorkmaz, 2007) is tuned with identical base gains, $\lambda_{x,y} = 5, \rho_{x,y} = 3, K_{x,y} = 1, \hat{d}^{\pm}_{x,y} = \pm 10$, as the

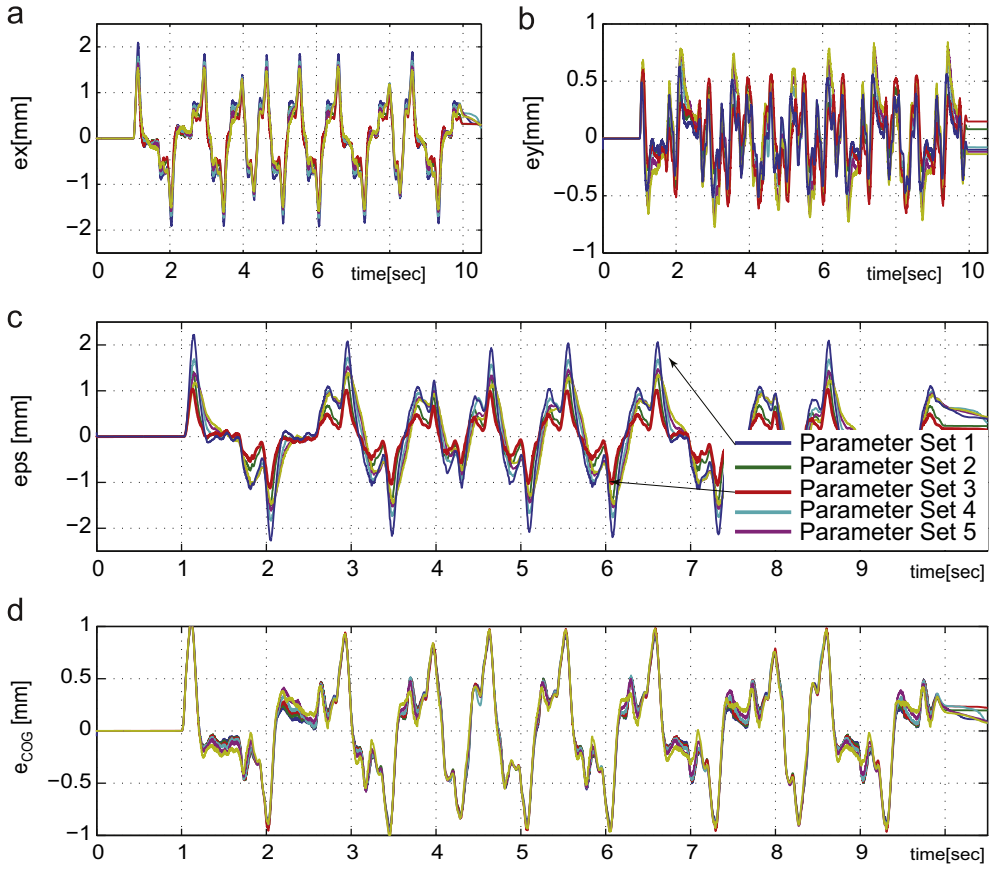

Fig. 10. Experimental tracking and synchronization response: (a) tracking errors of Motor X, (b) tracking errors of Motor Y and (c) synchronization errors, and (d) center of gravity motion errors.

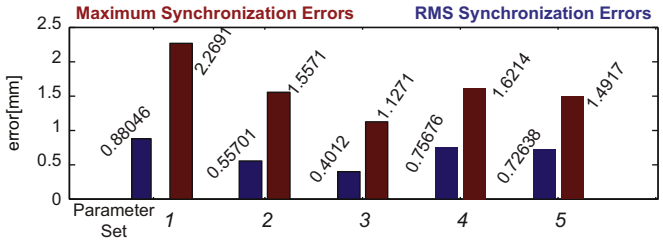

Fig. 11. Evaluation of the synchronization performance.

proposed controller to achieve a fair and moderate comparison. In the first experiment, *single tooth cutting* is performed (see Fig. 12b), and synchronization errors under conventional *master–slave* control and *tandem ASMC* are compared against the proposed controller. Cutting conditions are selected to be conventional where spindles rotate at 200 rev/min, and a steel plate in the size of 400 mm × 200 mm × 13.2 mm is fed at a speed of 800 mm/min. Each spindle removes 0.1 mm of thick material on each side of the hardened steel (JIS SS400) plate, which at max generates 300–500 N of cutting force. The cutter-work-piece engagement is detected by placing an accelerometer on the side of the workpiece (see Fig. 1b). Since cutting is repetitive, a section of the experiments is presented in Fig. 13. Synchronization performance of the controllers is compared in Fig. 13a–c. As shown, P-PI *master–slave* control presents the worst performance. The synchronization errors rise up to 30 counts with the engagement and fluctuate down to 25 counts after disengagement of the left and right tooth,

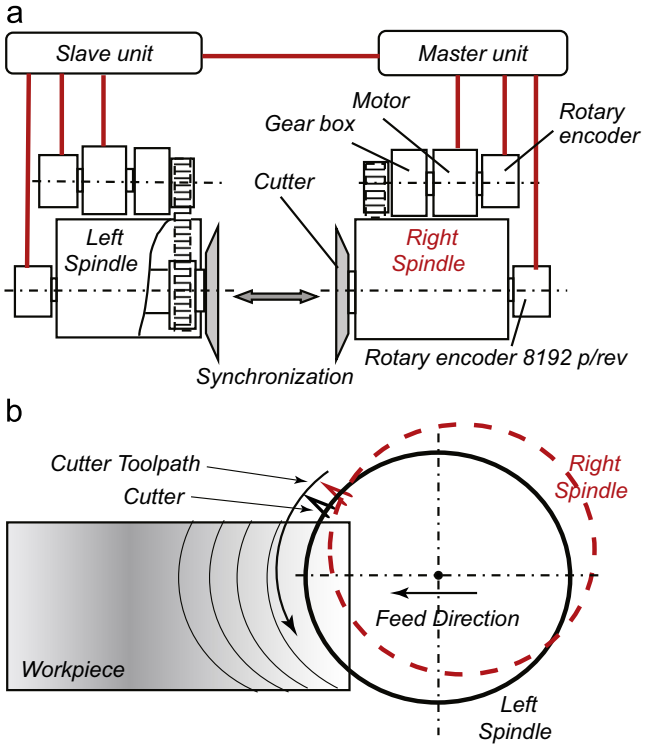

Fig. 12. Double-sided milling control system and cutting experiment: (a) double-sided milling machine master–slave control system and (b) cutting experiment.

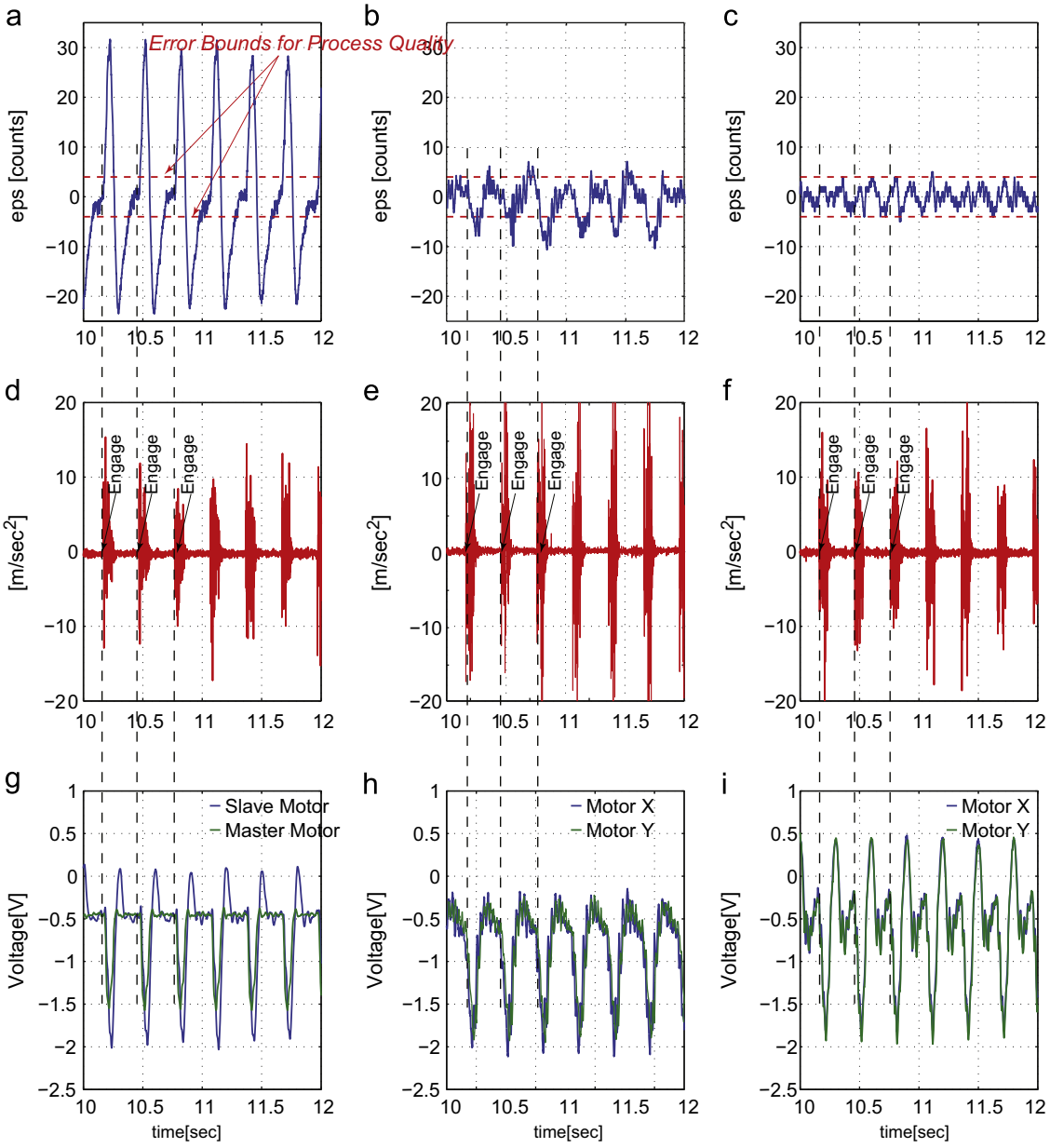

Fig. 13. Single tooth cutting experimental results. P-PI master–slave control: synchronization error (a), acceleration pick−up (d), motor X–Y Control Signal (g). Tandem ASMC (Kamalzadeh & Erkorkmaz, 2007): synchronization error (b), acceleration pick−up (e), motor X–Y control signal (h). Proposed control: synchronization error (c), acceleration pick−up (f), motor X–Y control signal (i).

which in return deteriorates the manufacturing quality. From the motor torque signal (Fig. 13g), it can also be seen that the slave motor follows the master with a lag of approximately 20 ms due to the master–slave design structure. Fig. 13b presents the synchronization errors under the ASMC control scheme. Similarly, synchronization errors occur as soon as the teeth engage/disengage the work-piece due to the fact that disturbances acting on the drives are not perfectly identical. However, robust disturbance rejection characteristics of the ASMC can keep synchronization errors smaller, in the range of ± 8 counts. Some control signal chattering and effect of noise can be observed. In both cases, 25–30% of the maximum motor load capacity is utilized during cutting. The performance of the proposed synchronizing sliding mode control is presented in Fig. 13c. As shown, proposed controller delivers the most accurate synchronization and keeps errors steady by robustly coupling the drives for synchronization objective. As a result, synchronization errors are kept within the manufacturing requirement of ± 4 counts at all times, which results in a more favorable surface finish quality. It should also be noted that, since synchronization errors are kept small and steady under the proposed control, even if process parameters such as the cutting speed, or depth is altered, the synchronization performance would not deteriorate, which could not be satisfied nor by the ASMC neither by the P-PI. Thus, proposed sliding mode controller introduces significant robustness and flexibility to the double-sided machining process.

Additionally, performance of the proposed controller on the process quality is confirmed by measuring the vibration marks left on the finished work-piece. Surface topography of a 20 mm $\times$ 30 mm section from the upper right corner of cut work-piece is taken and presented in Fig. 14. Surface topography of this small section is significant as it is dynamically compliant due to clamping and thus easy to vibrate if the teeth do not enter with precision synchronization into the material. The cutter's path can be seen on

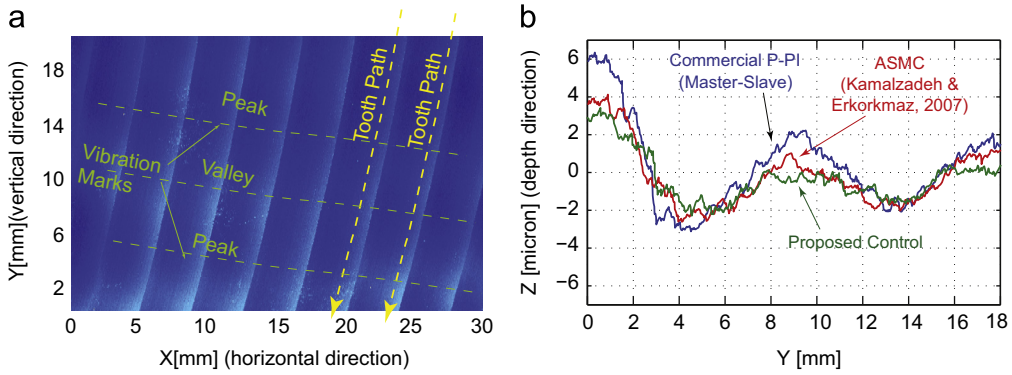

Fig. 14. Surface quality in single tooth cutting: (a) topography of the work-piece (sample section) and (b) relative vibration measured along cutter path.

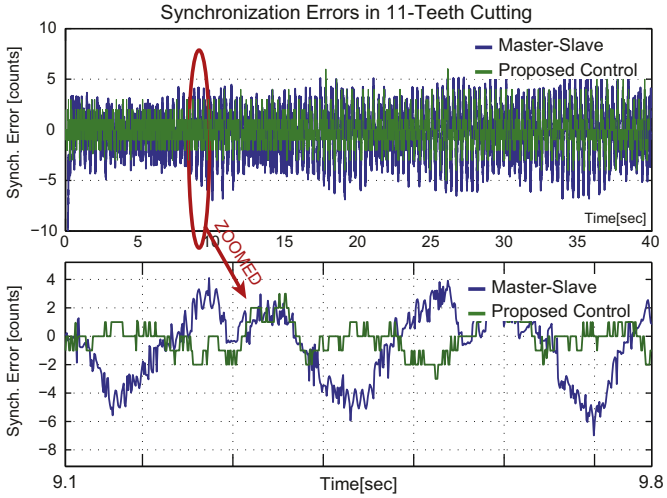

Fig. 15. Synchronization errors in 11-teeth double-sided cutting.

surface topography, and the cutting marks due to material removal are visible from Fig. 14a in the depth direction. Vibration occurs in the z (depth) direction, which is normal to the surface. The surface height is measured along the path of the tooth, and Fig. 14b shows the vibration amplitude along the tooth's path. It can be noted that the proposed controller reduces the vibration amplitude around 50% from 4 μm peek-to-peek down to 2 μm for the given experimental condition. This results in a better surface roughness and desired flatness in the finished product. A part from this particular experimental condition, when the spindle rotation speed is further increased, cutting with the *master–slave* or the *tandem ASMC* control would present even higher vibration marks since the settling time will be less after the cutter work-piece engagement. However, proposed contro\ller's performance would not decay.

In the second experiment, 11 teeth cutting is performed. In this condition due to the width of the plate several cutters are always in cut generating a physical coupling between X and Y spindles through the work-piece. Measured synchronization errors between the left and the right spindle are presented in Fig. 15. This condition essentially favors the master–slave control since physical coupling is provided by the work-piece and subsequent cutter engagement does not induce severe disturbance fluctuation. Even in this condition, proposed controller outperforms the master–slave by keeping synchronization errors only within several encoder counts. This proves the effectiveness of the proposed synchronization sliding mode controller in a practical manufacturing application.

6. Conclusions and final remarks

A continuous time sliding mode controller for motion synchronization between dual servo systems is proposed in this research. The proposed controller shows robust coupling and motion synchronization in dual servo systems against disturbances and un-modeled dynamics. Its performance is validated experimentally on a dual linear motor setup and also through implementation in a commercial manufacturing system by machining experiments. The controller presents practical implementation of the heavily researched Sliding Mode Controller theory using conventional PID blocks for the benefit of control engineer's practice. Particularly, the structured derivation of the control law allows variety of other motion systems such as dual motor driven feed drives or gantry type precision motion systems to benefit from the developed design scheme.

Acknowledgment

This research is sponsored by the Japan Society for Promotion of Science (JSPS). The authors would like to express their gratitude to Murata Machinery and Daido Amistar for their support in providing equipment and experimental facilities.

Appendix

The convergence of the errors by the proposed sliding mode control is expanded in this appendix. First, Lyapunov function (E) is postulated in Eq. (12) is lower bounded, and its derivative is forced to decrease by the control law in Eq. (19):

$$\lambda\mathbf{FM}\dot{\mathbf{e}} + \mathbf{FM}\ddot{\mathbf{x}}_{\mathbf{ref}} + \mathbf{FB}\dot{\mathbf{x}} + \mathbf{F}\hat{\mathbf{d}} + \mathbf{KS} = \mathbf{Fu}. \tag{A.1}$$

As a result, the sliding manifold $\mathbf{S}$, the error states $\mathbf{Fe}$,$\mathbf{F}\dot{\mathbf{e}}$ and the estimated disturbances $\hat{\mathbf{d}}$ are all bounded considering Eqs. (10) and (11). Substituting the control law (A.1) into the plant dynamics in Eq. (6) reveals

$$\begin{aligned}\mathbf{F}\ddot{\mathbf{e}} = {} & \mathbf{F}\ddot{\mathbf{x}}_{\mathbf{ref}} - \lambda\mathbf{F}\dot{\mathbf{e}} - \mathbf{F}\ddot{\mathbf{x}}_{\mathbf{ref}} - \mathbf{FM}^{-1}\mathbf{B}\dot{\mathbf{x}} - \mathbf{FM}^{-1}\hat{\mathbf{d}} \\ & - \mathbf{FM}^{-1}\mathbf{KS} + \mathbf{FM}^{-1}\mathbf{d} + \mathbf{FM}^{-1}\mathbf{B}\dot{\mathbf{x}}\end{aligned} \tag{A.2}$$

Re-arranging (A.2) leads to the following sliding manifold dynamics

$$\underbrace{\mathbf{F}\ddot{\mathbf{e}} + \lambda\mathbf{F}\dot{\mathbf{e}}}_{\dot{\mathbf{S}}} + \mathbf{M}^{-1}\mathbf{KS} = \mathbf{FM}^{-1}(\mathbf{d}-\hat{\mathbf{d}}) \rightarrow \dot{\mathbf{S}} + \mathbf{M}^{-1}\mathbf{KS} = \mathbf{FM}^{-1}(\mathbf{d}-\hat{\mathbf{d}}) \tag{A.3}$$

Eq. (A.3) shows that derivative of the sliding surface $\dot{\mathbf{S}}$ is bounded since $(\mathbf{d}-\hat{\mathbf{d}})$ is bounded. Thus, the second derivative of the Lyapunov function becomes also bounded by Eq. (17), i.e. $\ddot{E} = -2\mathbf{S}^T\mathbf{K}\dot{\mathbf{S}}$. In conclusion, E is positive definite lower bounded, $\dot{E}$ is negative definitive and $\ddot{E}$ is bounded, which proves that E is a

uniformly continuous function. Barbalat's lemma (Slotine & Li, 1991) dictates that $E \to 0$, $S \to 0$ as $t \to \infty$, which ensures that all the errors slide/converge to the origin. At last, considering the transformation **Fe**, it can also be concluded that tracking e_x, e_y and the synchronization errors $\varepsilon = e_x - e_y$ both converge to origin proving stability of the overall controller.

References

Altintas, Y. (2000). *Manufacturing automation: Metal cutting mechanics. Machine tool vibrations, and CNC design*. Cambridge University Press.

Altintas, Y., Erkorkmaz, K., & Zhu, H. W. (2000). Sliding mode controller design for high speed feed drives. *Annals of CIRP*, *49*(1), 265–270.

Bartolini, G., Ferrara, A., & Usai, E. (1998). Chattering avoidance by second-order sliding mode control. *IEEE Transactions on Automatic Control*, *43*(2), 241–246.

Chen, S-L., Liu, H-L., & Ting, S. C. (2007). Contouring control of biaxial systems based on polar coordinates. *IEEE/ASME Transactions on Mechatronics*, *7*(3), 329–345.

Chiu, T. C., & Tomizuka, M. (2000). Contouring control of machine tool feed drive systems: A task coordinate frame approach. *IEEE Transactions on Control Systems Technology*, *9*(1), 130–139.

De Carlo, R. A., Zak, S. H., & Matthews, G. P. (1988). Variable structure control of nonlinear multivariable systems: A tutorial. *Proceedings of the IEEE*, *76*(3), 212–232.

Erkorkmaz, K., & Altintas, Y. (2001). High speed CNC system design: Part II – Modeling and identification of feed drives. *International Journal of Machine Tools and Manufacture*, *41*(10), 1487–1509.

Franklin, F., Powell, J. D., & Emami-Naeini, A. (2009). *Feedback control systems* ((6th ed.). Prentice Hall.

Horowitz, R., Li, Y., Oldham, K., Kon, S., & Huang, X. (2003). Dual-stage servo systems and vibration compensation in computer hard disk drives. *Control Engineering Practice*, *15*(3), 291–305.

Jinbang, X., Wenyu, W., Anwen, S., & Yu, Z. (2013). Detection and reduction of middle frequency resonance for an industrial servo. *Control Engineering Practice*, *21*(7), 899–907.

Kamalzadeh, A., & Erkorkmaz, K. (2007). Accurate tracking controller design for high speed drives. *International Journal of Machine Tools and Manufacture*, *47*, 1393–1400.

Khan, M., Spurgeon, S., Levant, A. (2003), Simple output feedback 2-sliding controller for systems of relative degree two. In *Proceedings of the European control conference (ECC '03), Cambridge, UK*.

Koren, Y. (1991). Advanced controllers for feed drives. *CIRP Annals*, *41*(2), 689–698.

Koren, Y., & Lo, C. C. (1991). Cross-coupled biaxial computer control for manufacturing systems. *ASME Journal of Dynamic Systems, Measurement, and Control*, *102*, 265–272.

Levant, A. (1998). Robust exact differentiation via sliding mode technique. *Automatica*, *34*(3), 379–384.

Mori, T., Hiramatsu, T., & Shamoto, E. (2010). Simultaneous double-sided milling of flexible plates with high accuracy and high efficiency. *Precision Engineering*, *35*, 416–423.

Muske, K. R., Ashrafiuon, H., Nersesov, S., & Nikkhah, M. (2012). Optimal sliding mode cascade control for stabilization of underactuated nonlinear systems. *ASME Journal of Dynamics systems, Measurement and Control*, *134*(2), 1–11.

Okwudire, C. E., & Altintas, Y. (2009). Tracking error control of flexible ball-screw drives using a discrete-time sliding mode controller. *Journal of Dynamics Systems Measurement and Control, Transactions of ASME*, *131*(5).

Okwudire., C. E., & Altintas, Y. (2008). Dynamic stiffness enhancement of direct-driven machine tools using sliding mode control with disturbance recovery. *Annals of CIRP*, *58*(1), 335–338.

Peng, C. C., & Chen, C. L. (2007). Biaxial contouring control with friction dynamics using a contour index approach. *International Journal of Machine Tools and Manufacture*, *47*(10), 1542–1555.

Rodriguez-Angeles, A., & Nijmeijer, H. (2005). Synchronizing tracking control for flexible joint robots via estimated state feedback. *Journal of Dynamic Systems, Measurement and Control, Transactions of the ASME*, *126*(1), 162–172.

Sabanovic, A. (2011). Variable Structure systems with sliding modes in motion control – A survey. *IEEE Transactions on Industrial Informatics*, *7*(2), 212–223.

Sencer, B., & Altintas, Y. (2009). Modeling and control of contouring errors for five-axis machine tools. Part II – Precision contour controller design. *Transactions of ASME Journal of Manufacturing Science and Engineering*, *131*(3), 031007.

Shamoto, E., Mori, T., Nishimura, K., Hiramatsu, T., & Kurata, Y. (2010). Suppression of regenerative chatter vibration in simultaneous double-sided milling of flexible plates by speed difference. *CIRP Annals*, *59*(2), 387–390.

Sira-Ramirez, H. (1993). On the dynamical sliding mode control of nonlinear systems. *International Journal of Control*, *57*, 1039–1061.

Slotine, J. J., & Li, W. (1991). *Applied nonlinear control*. NJ: Prentice Hall.

Slotine, J. J. E., & Li, W. (1988). Adaptive manipulator control: A cast study. *IEEE Transactions on Automatic Control*, *33*(11), 995–1003.

Su, Y., Sun., D., Ren, L, & Mills, J. K. (2006). Integration of saturated PI synchronous control and PD feedback for control of parallel manipulators. *IEEE Transactions on Robotics*, *22*(1), 202–207.

Talole, S. E., & Phadke, S. B. (2008). Model following sliding mode control based on uncertainty and disturbance estimator. *ASME Journal of Dynamics systems, Measurement and Control*, *130*(3), 1–5.

Utkin, V. I. (1977). Variable structure systems with sliding modes. *IEEE Transactions on Automatic Control*, *22*(2), 212–222.

Won, M., & Hedrick, J. K. (2000). Disturbance adaptive discrete-time sliding control with application to engine speed control. *Journal of Dynamic Systems, Measurement and Control, Transactions of ASME*, *123*, 1–9.

Yeh, S.-S., & Hsu, P.-L. (2004). Perfectly matched feedback control and its integrated design for multiaxis motion systems. *Journal of Dynamic Systems, Measurement, and Control, Transactions of ASME*, *126*, 547–557.